Clays and Clay Minerals, Vol. 55, No. 6, 572–582, 2007.

SYNTHESIS OF Ni-RICH 1:1 PHYLLOSILICATES

MARIA BENTABOL[1], MARIA DOLORES RUIZ CRUZ[1,*] AND F. JAVIER HUERTAS[2]

[1]Departamento de Química Inorgánica, Cristalografía y Mineralogía, Facultad de Ciencias, Universidad de Málaga, Spain
[2] Estación Experimental del Zaidín, CSIC, Prof. Albareda 1, 18008 Granada, Spain

Abstract—Rapid dissolution of partly amorphized kaolinite in the systems kaolinite + $NiCl_2$, kaolinite + $Ni(OH)_2$, and kaolinite + $NiCl_2$ + $Ni(OH)_2$, at a temperature of 200ºC and at pH between 5.3 and 7.4, leads to the precipitation of Ni-poor kaolinite, Ni-rich kaolinite and Al-Ni-serpentine. Identification of the phases was carried out using a combination of X-ray diffraction and transmission/analytical electron microscopy. Ni-bearing kaolinite shows variable morphologies in the systems studied: stacks of kaolinite with relatively small Ni contents and fine-grained curved particles of Ni-rich kaolinite dominate in the Cl-bearing system; spherical particles with a disordered structure and relatively uniform Ni contents (in the order of 0.15 atoms per formula unit (a.p.f.u.)) and platy particles of Al-Ni-serpentine characterize the products formed in the $Ni(OH)_2$-richest systems. The presence of $Ni(OH)_2$ in the systems (with and without Cl) favors the dissolution process as well as rapid precipitation of spherical particles, and the formation of serpentine. A difference from Mg systems studied previously is a well defined phase intermediate in composition between kaolinite and serpentine which originated in the Ni-bearing systems. Increasing Ni content is clearly reflected in the parallel increase in the *b* cell parameter of kaolinite. The average composition of the coexisting Al-Ni-serpentine is: $(Al_{1.24}Ti_{0.01}Fe_{0.02}Ni_{1.31})$ $(Si_{1.58}Al_{0.42})O_5(OH,Cl)_2$.

Key Words—Al-Ni-serpentine, FTIR, Hydrothermal Synthesis, Ni-kaolinite, TEM/AEM, XRD.

INTRODUCTION

Kaolinite, dickite and nacrite show a very uniform chemistry: 46.5 wt.% SiO_2, 39.5 wt.% Al_2O_3, 14.25 wt.% H_2O, whereas halloysite has a similar Al:Si ratio but larger amounts of water. It is rare for these kaolin minerals to contain appreciable amounts of elements other than Si and Al. On the contrary, octahedral substitutions are common in 2:1 dioctahedral phyllosilicates (*e.g.* white mica), where cations such as Li^+, Fe^{2+}, Fe^{3+}, Mg^{2+}, Cr^{3+} and Ti^{4+} frequently substitute for Al^{3+} in the octahedral sheet (Newman and Brown, 1987). These cations are also potential candidates for substituting Al^{3+} in the kaolinite mineral structures. Ionic radii similar to Al^{3+} (Table 1) must theoretically favor the substitution, and indeed, some of these elements (*e.g.* Fe^{3+}, Cr^{3+}), with radii only slightly larger than Al^{3+} have been found in natural kaolinites (*e.g.* Brookins, 1973; Herbillon *et al.,* 1976; Maksimovic and Brindley, 1980; Mestdagh *et al.*, 1980; Cuttler, 1981; Maksimovic *et al.,* 1981; Stone and Torres Sánchez, 1988; Singh and Gilkes, 1991; Gaite *et al.,* 1993; Delineau *et al.,* 1994; Balan *et al.*, 1999, 2002). Nevertheless, the type of foreign cations present in the kaolinite structure is also dependent on the cation availability (bulk-rock composition). The amount of substitution appears to be controlled by the structure, the more disordered varieties accepting larger amounts of substitutions (Brindley *et al.,* 1986).

* E-mail address of corresponding author:
mdruiz@uma.es
DOI: 10.1346/CCMN.2007.0550604

Kaolinite which contains a considerable number of the cations (Table 1) has been synthesized; Fe-rich kaolinites were obtained by Angel *et al.* (1975), Petit and Decarreau (1990) and Iriarte *et al.* (2005) among others. Cu- and Ga-bearing kaolinites were synthesized by Angel *et al.* (1975), Meads and Malden (1975), Petit *et al.* (1995) and Martin *et al.* (1998). Mg-rich kaolinite was obtained by Bentabol *et al.* (2006). In most cases, the experiments were carried out starting from gels with appropriate compositions. Bentabol *et al.* (2006) used an alternative method, starting from partly amorphized kaolinite. The present work is part of a more extensive study, designed to investigate the capacity of kaolinite for hosting cations with relatively large ionic radii (Table 1), which had not been synthesized previously, for use as possible sinks for some trace elements (*e.g.* Cr, Ni, Co, Cu) in weathering profiles or hydrothermal alterations formed from basic or ultrabasic rocks. We present in this paper the results obtained from a set of hydrothermal reactions designed to favor the formation of Ni-kaolinite.

METHODOLOGY

Poorly crystalline kaolinite from Georgia (standard KGa-2, from The Clay Minerals Society Source Clays Repository), submitted to intense grinding, was used as the starting material. Details of the grinding method have been described previously (González Jesús *et al.*, 2000; Bentabol *et al.*, 2006). Grinding led to rounded particles with an average size <0.5 μm and to amorphization of a large proportion of the kaolinite. The impurities detected by X-ray diffraction (XRD) and transmission/analytical

Table 1. Ionic radii of some cations in octahedral coordination (Shannon, 1976).

Cation	Radius (Å)
Al^{3+}	0.54
Ti^{4+}	0.61
Cr^{3+}	0.62
Ga^{3+}	0.62
Fe^{3+}	0.65
Ni^{2+}	0.69
Mg^{2+}	0.72
Cu^{2+}	0.73
Co^{2+}	0.74

electron microscopy (TEM/AEM) consist of abundant grains of anatase and minor Fe oxide.

Three chemical systems (kaolinite + $NiCl_2$, kaolinite + $Ni(OH)_2$, and kaolinite + $NiCl_2$ + $Ni(OH)_2$) were studied at a temperature of 200ºC (Table 2). The hydrothermal treatments were conducted in 50 cm^3 Teflon-lined reactors (Parr 4744) which were maintained at a constant temperature of 200ºC (±3ºC). The solid products of the reactions (Table 3) were washed repeatedly and then characterized by XRD, Fourier transform infrared (FTIR) spectroscopy and TEM/AEM. The XRD patterns were obtained using a Philips X'Pert PRO MPD (Malaga University), with CuKα radiation, at 35 mA and 45 kV, with a step size of 0.01º2θ and a counting time of 2 s from 2 to 65º2θ for randomly oriented mounts.

The FTIR spectra, obtained from KBr pellets (2 wt.% sample) previously dried at 120ºC for 1 day, were carried out in a Nicolet spectrometer (20XB), and scanned in the range 4000−400 cm^{-1}. The resolution was 1 cm^{-1}. 400 scans were accumulated to improve the signal to noise ratio in the spectra.

The TEM study was carried out at the CIC (University of Granada), using a Philips CM-20 microscope operated at 200 kV (fitted with an ultrathin window, solid-state Si(Li) detector for energy dispersive X-ray analysis (EDAX)). The solid products were encased within an epoxy resin and then sliced. The atomic % was calculated by the Cliff-Lorimer thin-film ratio criteria (Lorimer and Cliff, 1976). The TEM images with higher resolution were obtained using a Jeol 3000 F, operated at 300 kV (University Complutense, Madrid).

Table 2. Reactions studied.

Reaction X: 1 Kln + 0.6 $NiCl_2$		Time
	X-1	1 day
	X-15	15 days
	X-30	30 days
Reaction XM: 1 Kln + 0.3 $NiCl_2$ + 0.3 $Ni(OH)_2$		
	XM-1	1 day
	XM-15	15 days
	XM-30	30 days
Reaction XT: 1 Kln + 0.6 $Ni(OH)_2$		
	XT-1	1 day
	XT-15	15 days
	XT-30	30 days

Solid:solution ratio = 1:15

RESULTS

XRD

The solid phases identified by XRD in the products of the several reactions were kaolinite and serpentine, except for reaction XT-1, where serpentine is absent and $Ni(OH)_2$ is abundant. A weak reflection at 4.08 Å, observed in some of the patterns (Figure 1) may be due to the presence of a small amount of opal. The solid products of the reaction X-30 lead to XRD patterns where two reflections, at 1.541 Å and 1.491 Å, reveal the presence of a dominant dioctahedral phase (kaolinite) and minor trioctahedral phase (serpentine). In the products of the reactions XM-30 and XT-30, three well defined reflections appear at this zone: a kaolinite reflection (at 1.489−1.491 Å), a serpentine reflection (at 1.543 Å) and an intermediate reflection, the spacings of which vary between 1.509 and 1.517 Å. This reflection was attributed to a phase with composition intermediate between kaolinite and serpentine. This intermediate phase was not observed in the Mg-bearing equivalent reactions (Bentabol *et al.*, 2006).

In the 02,11 region of the XRD patterns (19−24º2θ), the products of reactions X and XM show two defined reflections at 4.36 Å and 4.16 Å which were not observed in the patterns of Mg-bearing kaolinite (Bentabol *et al.*, 2006), indicating a greater degree of ordering in the Ni-bearing kaolinite. The patterns of the

Table 3. Products of the reactions.

	d_{060} (Kln)	d_{060} (Ni-Kln)	d_{060} (Srp)	Srp:Ni-Kln:Kln ratio*
Reaction X: Kln +Srp	1.491		1.543	3:0:20
Reaction XM: Kln + Srp	1.491	1.509	1.543	3:6:20
Reaction XT: Kln+Srp±$Ni(OH)_2$	1.489	1.517	1.543	7:8:20

* Ratio estimated from the relative intensity of the 060 reflections in the XRD patterns

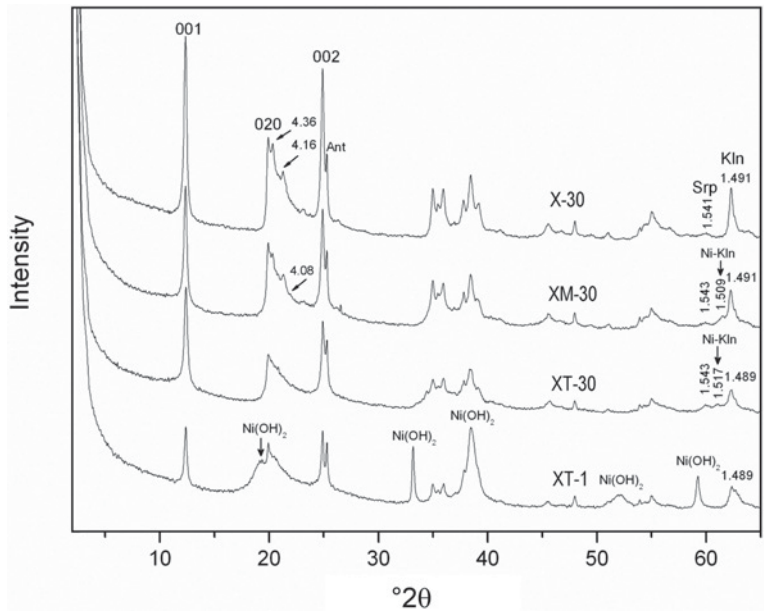

Figure 1. Representative XRD patterns obtained from unoriented samples (range 2−65º2θ) of the solid products of the hydrothermal reactions. Kln: kaolinite; Srp: serpentine; Ni-Kln: Ni-rich kaolinite. Ant: Anatase. CuKα radiation.

products of reaction XT are, however, characteristic of a very disordered kaolinite (Plançon and Zacharie, 1990).

TEM/AEM study

The products of reactions XT-1, XT-30 and XM-30 were selected for study by TEM/AEM. Low-magnification images of the products of the reactions XT-1 and XT-30 are characterized by the prevalence of spherical particles with kaolinite composition. Spherical particles are accompanied by thin particles of Ni hydroxide, similar to those described by Ni *et al.* (2006), in the products of reaction XT-1 only (Figure 2a). After a reaction time of 30 days the spherical particles coexist with minor stacks and platy particles of serpentine (Figure 2b).

Spherical particles from sample XT-1 generally show very small amounts of Ni (Table 4, analyses 1−3) whereas kaolinite from sample XT-30 shows a wide range of Ni contents (0.04−0.64 a.p.f.u.) (Table 4, analyses 4−10). Some analyses show, in addition to Ni, small amounts of Fe, probably from dissolution of Fe oxide present in the starting kaolinite. Figure 2b shows a typical platy particle of serpentine from sample XT-30. The analyses obtained from serpentine particles (Table 4, analyses 11−14) show some variation, affecting the tetrahedral substitution (^{IV}Al = 0.32−0.52 a.p.f.u.), the Ni content (1.17−1.37) and the total

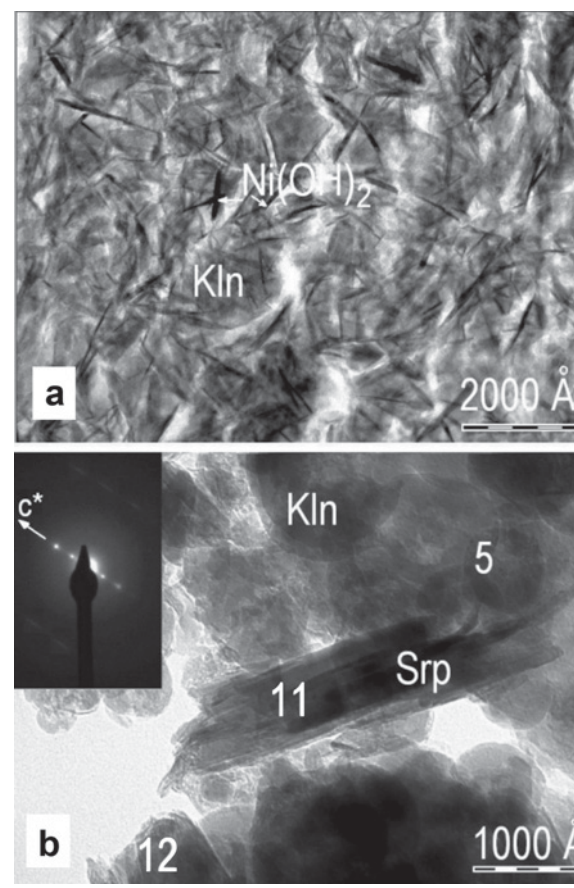

Figure 2 (*right*). (a) Low-magnification TEM image of the solid products of reaction XT-1, showing thin particles of $Ni(OH)_2$ with dark contrast, enclosed in a lighter matrix of finely-grained spherical particles. (b) Low-magnification image of the products of reaction XT-30, showing several Al-Ni-serpentine platy particles and spherical kaolinite. The numbers correspond to the analyses reported in Table 4. Kln: kaolinite; Srp: serpentine.

Table 4. AEM data for Ni-kaolinite and Al-Ni-Srp; cation contents in a.p.f.u.

	— Sample XT-1 —			Sample XT-30										
	1	2	3	4	5	6	7	8	9	10	11	12	13	14
Si	2.01	2.05	1.99	2.06	1.81	1.93	1.83	1.85	1.84	1.81	1.66	1.68	1.48	1.50
^{IV}Al	0.00	0.00	0.01	0.00	0.19	0.07	0.17	0.15	0.16	0.19	0.34	0.32	0.52	0.50
^{VI}Al	1.92	1.88	1.97	1.86	1.99	1.92	1.93	1.86	1.62	1.59	1.31	1.21	1.24	1.24
Ti	0.00	0.00	0.00	0.01	0.00	0.00	0.00	0.03	0.00	0.02	0.01	0.03	0.01	0.01
Fe	0.05	0.03	0.00	0.02	0.02	0.02	0.01	0.03	0.03	0.02	0.03	0.05	0.02	0.01
Ni	0.02	0.04	0.05	0.04	0.09	0.13	0.17	0.18	0.61	0.64	1.17	1.23	1.30	1.37
Σoct.	1.99	1.95	2.02	1.93	2.10	2.07	2.11	2.10	2.26	2.27	2.52	2.52	2.63	2.62

Sample XM-30																				
	15	16	17	18	19	20	21	22	23	24	25	26	27	28	29	30	31	32	33	34
Si	2.00	2.04	2.02	2.04	2.00	2.07	2.01	2.06	2.05	2.01	2.09	2.03	1.99	2.01	2.05	2.03	2.03	2.07	1.55	1.58
^{IV}Al	0.00	0.00	0.00	0.00	0.00	0.00	0.00	0.00	0.00	0.00	0.00	0.00	0.01	0.00	0.00	0.00	0.00	0.00	0.45	0.42
^{VI}Al	2.00	1.94	1.94	1.93	1.91	1.84	1.94	1.84	1.77	1.84	1.73	1.82	1.85	1.79	1.71	1.58	1.46	1.52	1.20	1.25
Fe	0.00	0.01	0.07	0.01	0.00	0.04	0.02	0.00	0.02	0.00	0.00	0.00	0.00	0.01	0.00	0.02	0.00	0.01	0.00	0.01
Mg	0.01	0.01	0.00	0.02	0.06	0.02	0.03	0.04	0.04	0.04	0.02	0.01	0.01	0.03	0.04	0.00	0.09	0.06	0.09	0.06
Ni	0.00	0.00	0.00	0.00	0.01	0.02	0.04	0.07	0.14	0.15	0.19	0.20	0.20	0.20	0.23	0.43	0.59	0.52	1.34	1.27
Σoct.	2.01	1.96	2.01	1.96	1.98	1.92	2.03	1.95	1.97	2.03	1.94	2.03	2.06	2.03	1.98	2.03	2.14	2.11	2.63	2.59
Cl	0.00	0.00	0.00	0.00	0.00	0.01	0.00	0.00	0.02	0.00	0.02	0.01	0.01	0.03	0.03	0.12	0.12	0.13	0.19	0.21

Analyses have been arranged in order of increasing Ni contents

octahedral occupancy (2.52−2.63), although all are Al-rich, and typical of a trioctahedral phase with an important dioctahedral component, with an average formula $(Al_{1.24}Ti_{0.01}Fe_{0.02}Ni_{1.31})(Si_{1.58}Al_{0.42})O_5(OH,Cl)_2$. This serpentine appears to be the Ni equivalent of the Al-Mg-serpentine associated with Mg-kaolinite (Bentabol *et al.*, 2006), which showed an average formula $(Al_{1.06}Fe_{0.03}Mg_{1.28}Ni_{0.18})(Si_{1.83}Al_{0.17})O_5(OH,Cl)_2$. Compared with brindleyite (Maksimovic and Bish, 1978), our Al-Ni serpentine has less octahedral occupancy.

Low-magnification images of the products of reaction XM-30 show two dominant types of morphologies: (1) large stacks of kaolinite with little Ni content and sizes >5000 Å thick (Figure 3a); and (2) fine-grained, frequently curved particles of a Ni-rich phase (Figure 3b). Very minor amounts of spherical particles were also observed. The large stacks appear to be made up of parallel or subparallel particles of variable thickness. The SAED patterns show, in some cases, a typical a^*-c^* kaolinite-like lattice (Figure 3a, inset), whereas in other cases, the SAED patterns reveal the presence of kaolinite particles with variable orientation, but sharing the c^* axis (Figure 3b, inset).

The AEM data obtained from the stacks (Table 4, analyses 15−26) reveal that several particles have a kaolinite composition, with very variable Ni contents (0.0−0.20 a.p.f.u.), although the particles forming the external zones of the stacks are enriched in Ni (Figure 3b). The analyses obtained in the fine-grained matrix that encloses the stacks (Table 4, analyses 27−29 and 31−32) show larger Ni contents (up to 0.59 a.p.f.u.). Most analyses of kaolinite display an excess of Si when the formulae are calculated on the basis of $O_5(OH)_4$. This excess may be derived from selective Al loss during the analyses. It is also possible that the excess Si reflects the possibility that the kaolinite particles are covered with a thin coating of amorphous silica, as observed by Jepson and Rowse (1975).

Table 4 and Figure 4 show increases in Cl contents with increasing Ni contents in the products of the reaction XM. Figure 4 shows three separate populations of analyses for Ni-bearing phases: (1) a population with small Cl (<0.05 a.p.f.u.) and Ni (+Fe+Mg) (0.0−0.28 a.p.f.u.) contents, corresponding to the stacks and spherical particles; (2) a population with larger Cl contents (0.10−0.18 a.p.f.u.) and Ni (+Fe+Mg) contents between 0.50 and 0.70 a.p.f.u., corresponding to the fine-grained curved particles; and (3) the serpentine population, with larger Ni contents (~1.40 a.p.f.u.). Serpentine formed in the Cl-free system (reaction XT) evidently does not contain Cl.

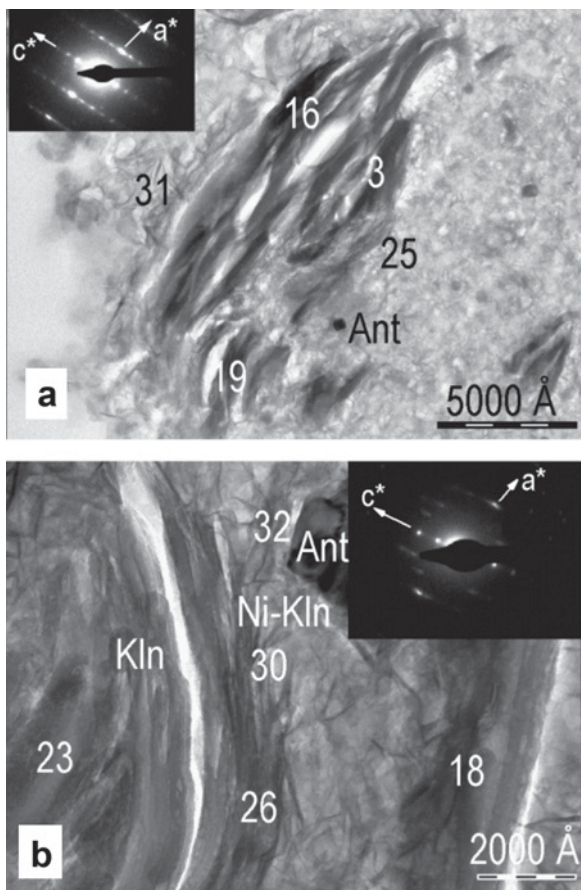

Figure 3. (a) Low-magnification TEM image of a typical kaolinite stack from sample XM-30, enclosed within a fine-grained matrix of Ni-rich particles. (b) Curved particles of Ni-rich kaolinite form the external zones of the stack and also appear as isolated curved particles. The SAED pattern of the stack (inset) reveals the presence of kaolinite particles with variable orientation and sharing the c^* axis. The numbers correspond to the analyses reported in Table 4. Kln: kaolinite; Ant: anatase.

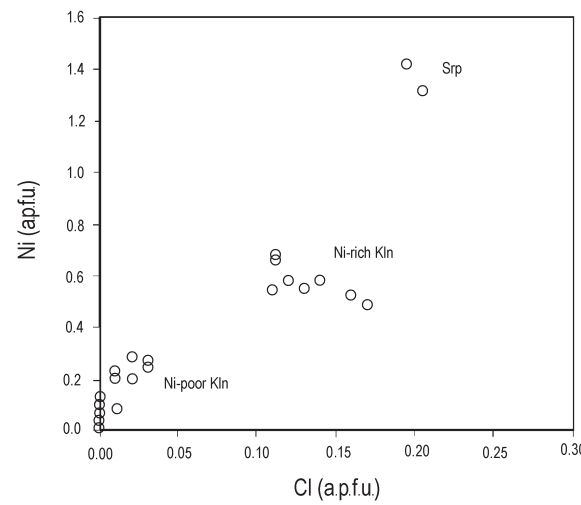

Figure 4. Chemical plot showing the positive correlation between Cl and Ni contents in kaolinite, Ni-kaolinite and Ni-serpentine.

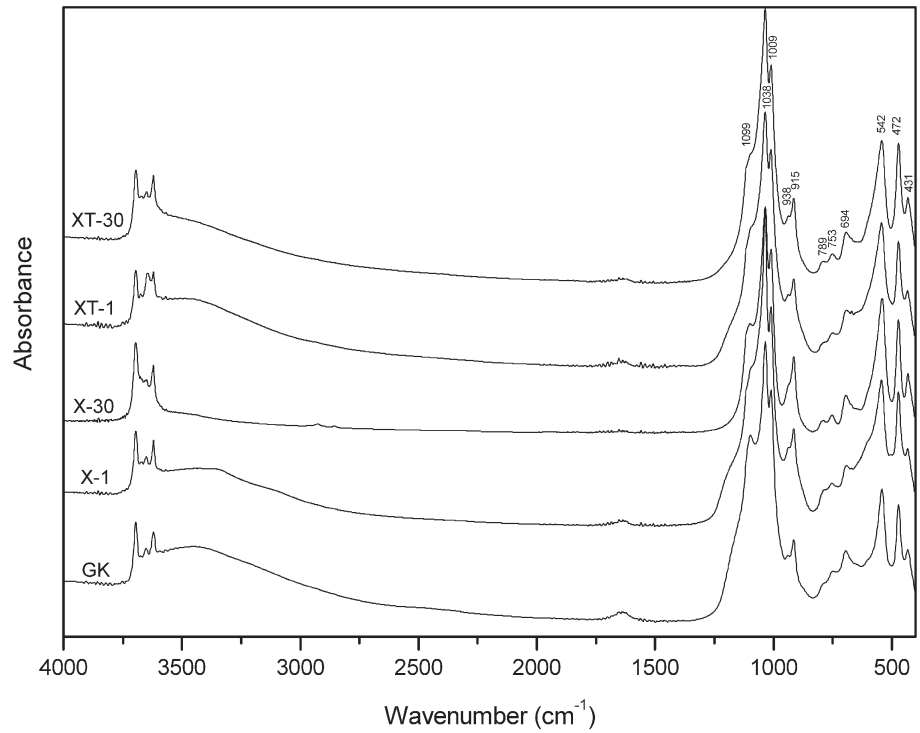

Figure 5. FTIR spectra of some selected products of the hydrothermal reactions and of the starting ground kaolinite (GK).

FTIR results

Some significant FTIR spectra of the products of the reactions are shown in Figure 5, together with the spectrum of the starting kaolinite. In the low-frequency region, the spectra of the synthetic phases are similar, both in terms of position and band intensity, to that of the starting kaolinite, whereas some interesting differences can be observed in the OH-stretching region (Figure 6). Figure 6 also includes the spectrum of $Ni(OH)_2$. A first group of bands (at 3695 cm^{-1}, 3670 cm^{-1}, 3650 cm^{-1} and 3620 cm^{-1}) corresponds to υAl_2-OH vibrations. At short reaction times (1 day), all spectra show a noticeable increase in intensity of the 3651 cm^{-1} band. This effect is due, in the case of the spectrum of sample XT-1 (Figure 6b), to the presence of $Ni(OH)_2$, as indicated by the splitting of the band; Ni hydroxide is, however, lacking in the other products, suggesting that the modifications observed in the spectra of the products formed at short times mainly reflect structural features, such as the possible presence of multi-layer sequences in the rapidly crystallized kaolinite (Brindley *et al.*, 1986). In addition, the spectra show two small bands at ~3592 and ~3567 cm^{-1}; the high-frequency one can be tentatively assigned to υAlNiOH, as in the case of Fe-bearing kaolinites (Mendelovici *et al.*, 1979; Petit and Decarreau, 1990; Delineau *et al.*, 1994; Iriarte *et al.*, 2005), whereas the 3557 cm^{-1} band can be ascribed to υNi_2OH.

At longer reaction times, the intensity of the 3651 cm^{-1} intermediate band decreases again (especially in the products of reaction X), leading to spectra typical of kaolinite, indicating that most stacks formed at increasing run times have a more ordered kaolinite structure.

Chemical data

The evolution of the pH values and the Si, Al and Ni (mmol/L) contents in the solutions of the several reactions, including initial solutions, are shown in Table 5. The initial pH values (5.32−7.37) clearly depend on the $Ni(OH)_2$ content in the systems. These values show a rapid decrease after 1 day of reaction time (2.36−5.54) and a subsequent stabilization. The final pH values are clearly acidic, ranging from 1.96 (reaction X) to 5.33 (reaction XT).

The three sets of reactions also show a parallel evolution of the Ni contents, with a rapid initial decrease (at reaction times <1 day) that reveals the rapid incorporation of Ni in the solid products of the reactions. The Si and Al contents increase notably after 1 day whereas they display limited variations at increasing reaction times. This behavior reflects kaolinite dissolution and the almost immediate precipitation of the new phases.

DISCUSSION

The rapid dissolution of kaolinite in the systems kaolinite + $NiCl_2$, kaolinite + $Ni(OH)_2$, and kaolinite + $NiCl_2$ + $Ni(OH)_2$ releases to solution Si and Al that at

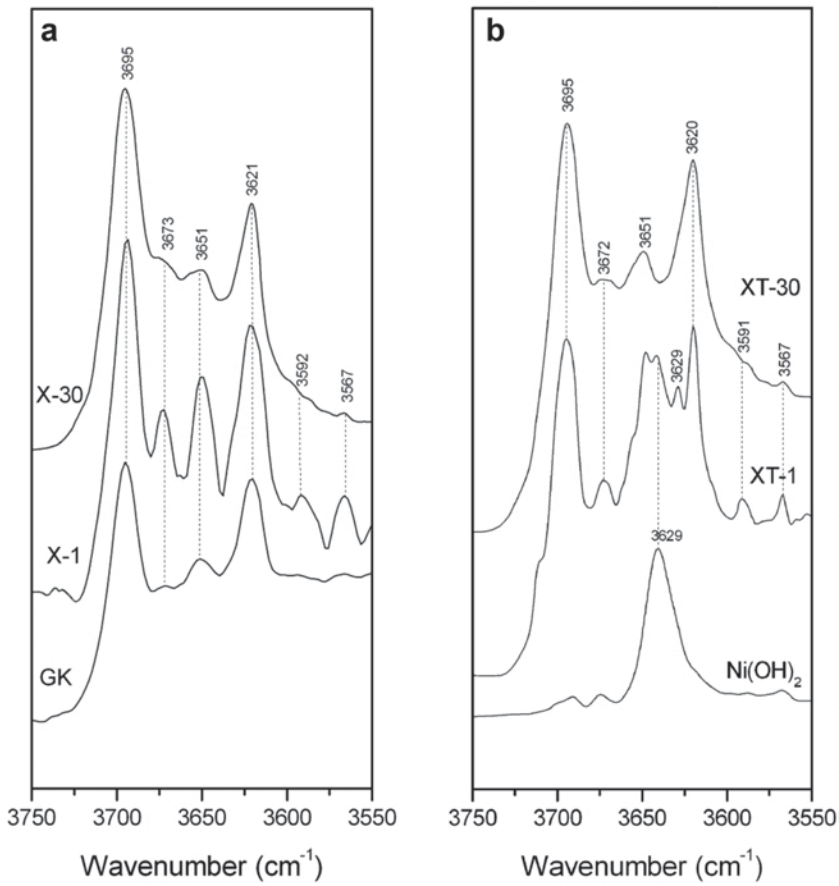

Figure 6. OH-stretching zone of the spectra shown in Figure 5. (a) Products of the reaction X. (b) Products of the reaction XT. The spectra of the starting kaolinite (GK) and of the $Ni(OH)_2$ have been included in a and b, respectively, to allow comparison.

200ºC led to the rapid precipitation of Ni-poor spherical particles with kaolinite composition and Ni hydroxide. At longer reaction times, this early assemblage evolves towards Ni-richer kaolinite and Al-Ni-serpentine.

The nature and significance of the spherical morphology in kaolinite has been debated since the work by Tomura *et al.* (1983). Although the lattice-fringe images have revealed in some cases the presence of radially arranged sectors of planar crystallites (*e.g.* Huertas *et al.*, 2004), the images of our spherical particles (Figure 7a) clearly reveal that they are composed of continuous curved layers, with a curvature radius of the

Table 5. pH and composition (mmol/L) of the solutions (Cl was estimated using the stoichiometry of the reactions).

Reaction	Time	pH	Si	Al	Ni	Cl
X	0	5.32	0.00	0.00	158.48	317
	1	2.36	97.80	24.68	19.74	317
	15	1.88	87.42	19.68	18.34	317
	30	1.96	86.97	14.68	18.65	317
XM	0	6.41	0.00	0.00	156.03	156
	1	3.18	76.28	15.06	8.70	156
	15	2.82	82.30	14.27	9.17	156
	30	3.00	78.69	18.34	9.14	156
XT	0	7.37	0.00	0.00	153.59	–
	1	5.54	62.71	4.87	4.17	–
	15	4.94	53.44	4.79	8.77	–
	30	5.33	48.37	2.19	7.16	–

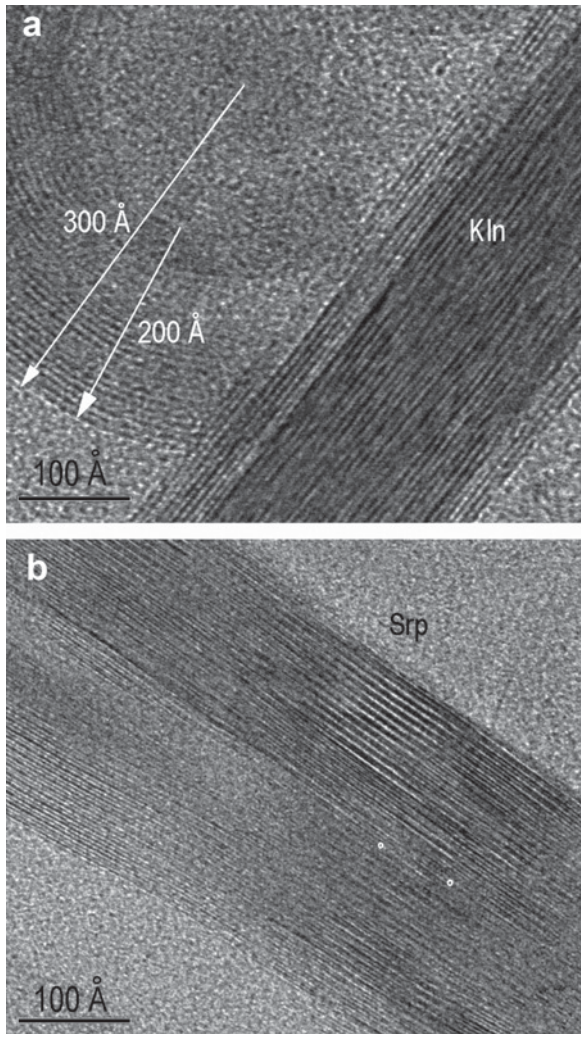

Figure 7. Lattice-fringe images of the products of reaction XT-30. (a) The platy particle of kaolinite grew, in appearance, from the earliest spherical particle. The spherical particle consists of concentric curved layers and an innermost part of poorly-crystalline material. (b) This serpentine particle consists of two packets which show a semi-coherent boundary. Small circles mark the interface dislocations.

order of 300 Å and an inner part consisting of poorly crystalline material with kaolinite composition. Since the analyses of these particles show Si contents $\geqslant 2$ a.p.f.u., it seems clear that curvature is not due to differences in size between the tetrahedral and octahedral sheets caused by tetrahedral substitutions, as in the case of halloysite, but probably to the presence (perhaps alternation) of layers with slightly different cell parameters or with different stacking sequences, as also suggested by the FTIR spectra. The lattice-fringe images of Al-Ni serpentine show, on the contrary, the prevalence of platy particles (Figure 7b). It can be deduced that the observed tetrahedral Al-for-Si substitutions in serpentine (0.30–0.50 a.p.f.u.) are large enough to produce a good fit between both sheets, leading to planar structures.

The EQ3/6 software for geochemical reaction and speciation (Wolery, 1992) was used to establish the fate of Ni and the precipitation of solid phases in the systems. The results should be used as a proxy of the system, as no thermodynamic data for the Ni-kaolinite phases were available. Modeling was performed using the solution compositions included in Table 5. According to EQ3/6, initial solutions at room temperature were undersaturated in all solid phases. As temperature is increased to 200ºC, initial solutions become supersaturated in Ni (oxy)-hydroxide and pH decreases due to Ni(II) hydrolysis. These changes induce precipitation of $Ni(OH)_2$, identified by TEM in the solid products, and a decrease in Ni(II) concentration. Acidic conditions induce dissolution of starting, low-crystallinity kaolinite and the release of Si and Al to solution. The saturation state of the solutions at time 1, 15 and 30 is very similar for each reaction system. Solutions of reaction X are close to equilibrium with respect to kaolinite and $Ni(OH)_2$, in agreement with the small variations of Si, Al and Ni concentrations. The results of the modeling are quite similar for the three reactions studied. Solutions from reactions XM and XT, with a pH more basic than those of reaction X, are more supersaturated in Ni oxy-hydroxides at short reaction times as they are less soluble at these pH values. There are no other notable features.

The assemblage Ni-kaolinite + Ni-Al-serpentine is similar to that obtained for the equivalent Mg-bearing systems (Bentabol *et al.*, 2006). Nevertheless, in the systems described in this paper, a phase with an intermediate composition between kaolinite and serpentine is also present. The significance of this phase is not clear. It could be interpreted as an intermediate metastable phase, which would evolve at longer run times towards kaolinite + serpentine. Nevertheless, the evolution of the solid products of the reaction XT at increasing run times (Figure 8) reveals that this phase becomes progressively better defined, whereas the relative kaolinite content decreases slightly, suggesting that the phase in equilibrium with the Al-Ni-serpentine is the most Ni-rich kaolinite.

Table 6 shows the values of the *b* cell parameter of kaolinite and serpentine and the mean Ni content measured in the two populations of kaolinite from samples XT-30 and XM-30. The exact determination of the spacing of the 06,33 reflection of kaolinite in the several reactions was carried out using the 101 reflection of anatase as an internal standard. The values determined in the Mg-bearing systems (Bentabol *et al.*, 2006) and in the Fe-bearing systems (Iriarte *et al.*, 2005) are also shown for comparison. The graphical plot of these values (Figure 9) reveals three different trends. Mg-bearing kaolinite shows a rather small increase of the *b* cell parameter at increasing substitution. Ni-kaolinite shows, on the contrary, a clear increase in the *b* cell

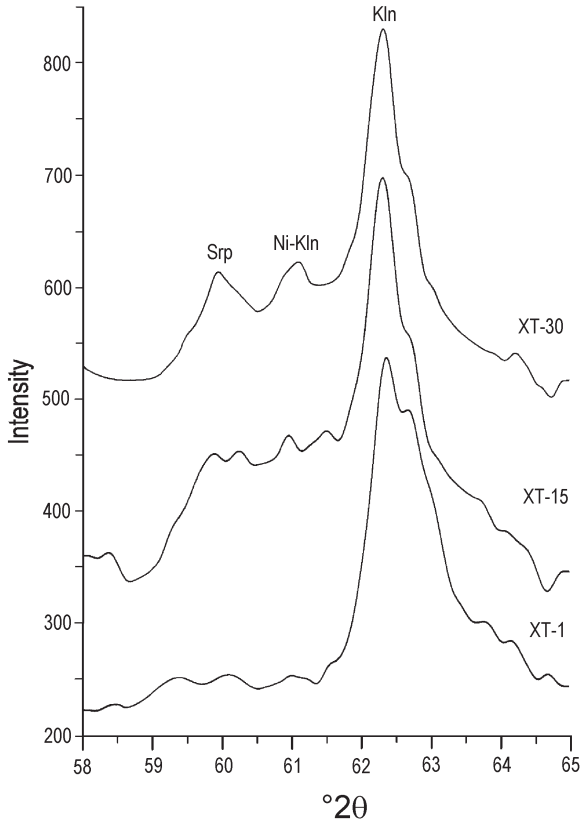

Figure 8. XRD patterns (in the range 58−65º2θ) of the products of reaction XT, showing the evolution of the composition of the newly formed phases at increasing reaction times. CuKα radiation.

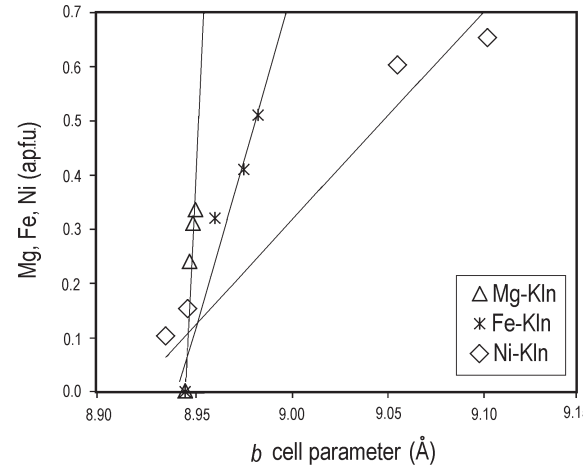

Figure 9. Plot of Mg, Fe and Ni contents (a.p.f.u.) *vs*. the *b* cell parameter in Mg-kaolinite (Bentabol *et al.*, 2006), Fe-kaolinite (Iriarte *et al.*, 2005) and Ni-kaolinite (this study).

parameter (Fig. 9) at increasing isomorphic substitution. Fe^{3+}-kaolinites occupy an intermediate position. These trends suggest that the presence of Fe^{3+} and especially of Ni^{2+} in the octahedral sheet increases the *b* cell parameter to a larger extent than Mg, as also observed in serpentine and micas (Brown and Brindley, 1980).

Ni-bearing kaolinite and serpentine show a clear correlation between the Cl and Ni contents (see Figure 4), indicating that Ni substitution favors the parallel Cl-for-OH replacement. Nevertheless, the maximum Cl-for-OH substitution appears to be limited at values <0.25 a.p.f.u. in the serpentine structure.

It is difficult to evaluate the stability of Ni-bearing kaolinite in natural environments since Ni is rare in the most common rock types. Previous data on Cr-bearing kaolinites (Brookins, 1973; Maksimovic and Brindley, 1980; Maksimovic *et al.,* 1981; Singh and Gilkes, 1991; Balan *et al.*, 2002) suggest, however, that Ni-kaolinite could be found associated with the alteration of Ni ores in ultramafic rocks. Since Ni-rich serpentine (brindleyite) is also a rare mineral, formed in Al-rich environments (Maksimovic and Bish, 1978), it is expected that the presence of high concentrations of both Al and Ni in solution are necessary for the formation of the assemblage Ni-kaolinite + Al-serpentine.

CONCLUSIONS

The hydrothermal reaction of partly amorphized kaolinite (at 200ºC) in the presence of Ni-bearing solutions yielded the assemblage Ni-poor kaolinite +

Table 6. *b* cell parameter of kaolinite and serpentine in the various reactions.

	Reaction	b_{kln} (Å)	b_{Srp} (Å)	Fe+Ni+Mg (a.p.f.u.)	References
Ni-Kln	X-30	8.946	9.246		This study
	XM-30	8.947+9.054	9.258	0.15−0.60	This study
	XT-30	8.934+9.102	9.258	0.10−0.65	This study
Mg-Kln	T-30	8.947		0.24	Bentabol *et al.* (2006)
	TM-30	8.950		0.33	Bentabol *et al.* (2006)
	TC-3	8.949		0.31	Bentabol *et al.* (2006)
Fe-Kln	KAF28	8.960		0.32	Iriarte *et al.* (2005)
	KAF42	8.976		0.41	Iriarte *et al.* (2005)
	KAF54	8.984		0.51	Iriarte *et al.* (2005)

Ni-rich kaolinite + Ni-Al-serpentine. The notable increase in the *b* cell parameter of kaolinite at increasing isomorphic substitutions confirms that the divalent cation Ni^{2+} substitutes for Al^{3+} in the octahedral sheet of the kaolinite. Rapid precipitation produced very disordered spherical structures at short reaction times, especially in the Cl-free system. These metastable phases evolve, at longer reaction times, towards kaolinite stacks.

Incorporation of large amounts of Ni (and other cations) in synthetic kaolinites indicates that the kaolinite structure is more flexible than previously assumed from the analyses of natural samples formed through alteration of acidic rocks. The assemblage Ni-kaolinite + Ni-Al-serpentine, which has not been described in natural environments, would probably require unusual Al- and Ni-rich chemical systems.

ACKNOWLEDGMENTS

The authors are grateful to Drs A. Bauer, C. Fialips, and B. Lanson whose suggestions and corrections improved the manuscript, and to M.M. Abad for help in obtaining the TEM/AEM data. This study received financial support from the Project CGL 2006-02481 (Ministerio de Educación y Ciencia) and from the Research Group RNM-199.

REFERENCES

Angel, B.R., Richards, K. and Jones, J.P.E. (1975) The synthesis, morphology, and general properties of kaolinites specifically doped with metallic ions, and defects generated by irradiation. *Proceedings of the International Clay Conference* 1975, 297–304.

Balan, E., Allard, T., Boizot, B., Morin, G. and Muller, J.P. (1999) Structural Fe^{3+} in natural kaolinites: New insights from electron paramagnetic resonance spectra fitting at X and Q-band frequencies. *Clays and Clay Minerals*, **47**, 605–616.

Balan, E., Allard, T., Morin, G. and Calas, G. (2002) Incorporation of Cr^{3+} in dickite: a spectroscopic study. *Physics and Chemistry of Minerals*, **29**, 273–279.

Bentabol, M., Ruiz Cruz, M.D., Huertas, F.J. and Linares, J. (2006) Hydrothermal synthesis of Mg-rich and Mg-Ni-rich kaolinite. *Clays and Clay Minerals,* **54,** 667–677.

Brindley, G.W., Chih-Chun, Kao, Harrison, J.L., Lipsicas, M. and Raythatha, R. (1986) Relation between structural disorder and other characteristics of kaolinites and dickites. *Clays and Clay Minerals*, **34**, 239–249.

Brookins, D.G. (1973) Chemical and X-ray investigation of chromiferous kaolinite ('miloschite') from the Geysers, Sonoma County, California. *Clays and Clay Minerals*, **21**, 421–422.

Brown, G. and Brindley, G.W. (1980) X-ray diffraction procedures for clay mineral identification. Pp. 305–360 in: *Crystal Structures of Clay Minerals and their X-ray Identification* (G.W. Brindley and G. Brown, editors). Monograph **5,** Mineralogical Society, London.

Cuttler, A.H. (1981) Further studies of ferrous iron doped synthetic kaolin: dosimetry of X-ray induced effects. *Clay Minerals*, **16**, 69–80.

Delineau, T., Allard, T., Muller, J.P., Barrès, O., Yvon, J. and Cases, J.M. (1994) FTIR reflectance *vs*. EPR studies of structural iron in kaolinites. *Clays and Clay Minerals*, **42**, 308–320.

Gaite, J.M., Ermakoff, P. and Muller, J.P. (1993) Characterization and origin of two Fe^{3+} EPR spectra in kaolinite. *Physic and Chemistry of Minerals*, **20**, 242–247.

González Jesús, J., Huertas, F.J., Linares, J. and Ruiz Cruz, M.D. (2000) Textural and structural transformations of kaolinites in aqueous solutions at 200ºC. *Applied Clay Science*, **17**, 245–263.

Herbillon, A.J., Mestdagh, M.M., Vielvoye, L. and Derouane, E. (1976) Iron in kaolinite with special reference to kaolinite from tropical soils. *Clay Minerals*, **11**, 201–220.

Huertas, F.J., Fiore, S. and Linares, J. (2004) *In situ* transformation of amorphous gels into spherical aggregates of kaolinite: A HRTEM study. *Clay Minerals*, **39**, 423–431.

Iriarte, I., Petit, S., Huertas, F.J., Fiore, S., Grauby, O., Decarreau, A. and Linares, J. (2005) Synthesis of kaolinite with a high level of Fe^{3+} for Al substitution. *Clays and Clay Minerals*, **53**, 1–10.

Jepson, W.B. and Rowse, J.B. (1975) The composition of kaolinite; an electron microscope microprobe study. *Clays and Clay Minerals*, **23**, 310–317.

Lorimer, G.W. and Cliff, G. (1976) Analytical electron microscopy of minerals. Pp. 506–519 in: *Electron Microscopy in Mineralogy* (H.R. Wenk, editor). Springer-Verlag, Berlin.

Maksimovic, Z. and Bish, D.L. (1978) Brindleyite, a nickel-rich aluminous serpentine mineral analogous to berthierine. *American Mineralogist*, **63**, 484–489.

Maksimovic, Z. and Brindley, G.W. (1980) Hydrothermal alteration of a serpentinite near Takovo, Yugoslavia, to chromium-bearing illite/smectite, kaolinite, tosudite and halloysite. *Clays and Clay Minerals*, **28**, 295–302.

Maksimovic, Z., White, J.L. and Logar, M. (1981) Chromium-bearing dickite and chromium-bearing kaolinite from Teslic, Yugoslavia. *Clays and Clay Minerals*, **29**, 213–218.

Martin, F., Petit, S., Decarreau, A., Ildefonse, P., Grauby, O., Beziat, D., Parseval, P. and Noack, Y. (1998) Ga/Al substitution in synthetic kaolinites and smectites. *Clay Minerals*, **33**, 231–241.

Meads, R.E. and Malden, P.S. (1975) Electron-spin resonance in natural kaolinites containing Fe^{3+} and other transition metal ions. *Clay Minerals*, **10**, 313–345.

Mendelovici, E., Yarif, S.H. and Villalva, R. (1979) Iron-bearing kaolinite in Venezuelan laterites; I. Infrared spectroscopy and chemical dissolution evidence. *Clay Minerals*, **14**, 323–331.

Mestdagh, M.M., Vielvoye, L. and Herbillon, A.J. (1980) Iron in kaolinite. II. The relationship between kaolinite crystallinity and iron content. *Clay Minerals*, **15**, 1–13.

Newman, A.C.D. and Brown, G. (1987) The chemical constitution of clays. Pp. 1–128 in: *Chemistry of Clays and Clay Minerals*. Monograph **6**, Mineralogical Society, London.

Ni, X., Zhao, Q., Li, B., Cheng, J. and Zheng, H. (2006) Interconnected β-$Ni(OH)_2$ sheets and their morphology-retained transformation into mesostructured Ni. *Solid State Communications*, **137**, 585–588.

Petit, S. and Decarreau, A. (1990) Hydrothermal (200ºC) synthesis and crystal chemistry of iron-rich kaolinites. *Clay Minerals*, **25**, 181–196.

Petit, S., Decarreau, A., Mosser, C., Ehret, G. and Grauby, O. (1995) Hydrothermal synthesis (250ºC) of copper-substituted kaolinites. *Clays and Clay Minerals*, **43**, 482–494.

Plançon, A. and Zacharie, C. (1990) An expert system for the structural characterization of kaolinites. *Clay Minerals*, **25**, 249–260.

Shannon, R.D. (1976) Revised effective ionic radii and systematic studies of interatomic distances in halides and chalcogenides. *Acta Crystallographica*, **A32**, 751–767.

Singh, B. and Gilkes, R.J. (1991) Weathering of a chromian

muscovite to kaolinite. *Clays and Clay Minerals*, **39**, 571–579.

Stone, W.E.E. and Torres Sánchez, R.M. (1988) Nuclear magnetic resonance spectroscopy applied to minerals. Part 6. Structural iron in kaolinite as viewed by proton magnetic resonance. *Journal of the Chemical Society, Faraday Transactions*, **84**, 117–132.

Tomura, S., Shibasaki, Y., Mizuta, H. and Kitamura, M. (1983) Spherical kaolinite: synthesis and mineralogical properties. *Clays and Clay Minerals*, **31**, 413–421.

Wolery, T.J. (1992) *EQ3/6, a software package for geochemical modeling of aqueous systems*. Lawrence Livermore National Laboratory, USA.

(*Received 22 January 2007; revised 14 August 2007; Ms. 1254; A.E. Bruno Lanson*)